공학석사학위논문

타이어 모델을 사용한
자율 드리프트 주행 제어 설계 및 분석

Autonomous Drift-Driving Control Design and Analysis with Nonlinear Tire-Model

2019 년 2 월

서울대학교 대학원

기계항공공학부

정 락 준

Abstract

Autonomous Drift-Driving Control Design and Analysis with Nonlinear Tire-Model

Rakjoon Chung
Mechanical & Aerospace Engineering
The Graduate School
Seoul National University

Control design and analysis of Wheeled Mobile Robot(WMR) autonomous drift-driving and the simulation experiment using the CarSim simulator are presented and the analysis of the controller proceeds. We first introduce WMR dynamics, tire model and problem formulation of the WMR. We then design drift-driving control using human strategy (control side slip angle and yaw rate). The drift-driving control consists of high-level control, optimization to find desired control input and high-gain control. We analyze the uncontrolled velocity dynamics and stability of the controller. The CarSim simulation results of drift-driving on steady-state equilibriums and the hairpin path with the desired yaw rate are provided.

Key Words: Wheeled Mobile Robot, Drift-driving control, Tire-model, Optimization, High-gain control, Jacobian linearization
Student Number: *2017-23468*

Contents

List of Figures

List of Tables

Abbreviations

WMR	**W**heeled **M**obile **R**obot
LQR	**L**inear **Q**uadratic **R**egulator
DoF	**D**egree **o**f **F**reedom

Chapter 1

Introduction

1.1 Motivation and related works

The Wheeled Mobile Robot (WMR) is often used in a variety of tasks due to its versatility and high stability. The WMR, therefore, has been studied widely [1–9]. In order to increase the working efficiency, the WMR is necessary to develop the movement at high speed. However, a controller that takes the slip at the wheels into account is needed since high speed of movement can generate slip at the wheels.

There are algorithms to predict and prevent the slip of the wheels in the path planning stage in order to perform the task in fast and non-slip condition. A control framework to enable WMR to autonomously drive with fast speed

without slip at the wheels was proposed in [10]. In addition, planning to generate a non-slip trajectory with time information and a controller for tracking the timed trajectory was implemented. The framework to determine slippage and roll-over tendency from calculating friction force and ZMP(zero-moment-point) from the given trajectory using third dimension dynamics was proposed in [11]. These algorithms prevent slipping and roll-over situations and help to move fast with non-slip condition, these algorithms did not use a slip of wheels.

The driving using the slip of wheels helps not only to move fast but also to prevent move off the track when it has a lower coefficient of friction like icy, snowy and rainy roads. Thanks to the friction coefficient can be estimated in real time [12], the friction force according to the slip can be estimated even if the frictional force is changed, and controllers can be performed using the friction forces.

The drift-driving is a method of moving sideways by using the slip of wheels, and the drift-driving uses the tire slip a lot. The drift-driving has been studied [13–18].

The 4-wheeled mobile robot dynamics, tire model and the limited slip differential are applied to model dynamics, and obtain equilibrium points of dynamics and compare the equilibrium points with real expert experiment data, and linearize the model dynamics and use the LQR(linear quadratic regulator) and backstepping control for steady-state drifting [13]. The 2-wheeled mobile robot dynamics and tire model used to find equilibrium values, and stabilize analysis

with the invariant set, and the controller was implemented with a RWD by-wire testbed in [14]. The steady-state equilibrium changes while drift-driving [15]. The path was generated from mixed with simplified and high fidelity dynamics for efficiency. The control choose open-loop and closed loop(LQR) base on predicted tracking error for drift-driving in [16].

1.2 Contribution of this work

In this thesis, we propose a drift-driving controller which does not directly use the values of equilibrium point or reference trajectory, unlike other controllers. We use human strategy to control only the direction of WMR which is related to the side slip angle and yaw rate. We control these values through cost optimization. The advantage of the proposed controller is that the controller can be applied in a variety of path since the equilibrium and reference are not defined. This designed controller allows the WMR to drive steady-state drift based on the analyzed velocity stability. This drift-driving control design allows path following because the controller does not use any equilibrium point values.

We use the single-track model dynamics and the forces from the tire model which determine the force between the wheel and the ground, and we discuss the problems in using these dynamics in Chapter 2. In Chapter 3, we design a drift-driving controller consists of high-level control, optimization to find steering control input and desired rear-wheel angular velocity, and high-gain control to

obtain rear-wheel torque for rear-wheel angular velocity. We analyze the uncontrolled velocity dynamics and controller in Chapter 4. The CarSim simulation results of using the proposed control are provided in Chapter 5.

Chapter 2

System Modeling

2.1 Model dynamics

To analyze the dynamics of the WMR, we apply a single-track dynamics model that approximates the entire dynamics of WMR to a two-wheel model that contains one front wheel and one rear wheel. This model is depicted in Fig. 2.1 where $(v, \beta, \theta, \delta) \in \Re$ are the WMR's velocity, side slip angle of mass center, yaw angle of mass center and the steering angle of the front wheel, respectively. The WMR is a rear-wheel-drive model and the WMR has three degrees of freedom as $(x, y, \theta) \in \Re$ which are spatial x-axis, y-axis position, and yaw angle. The dynamics of WMR is expressed in the body-fixed frame as follows.

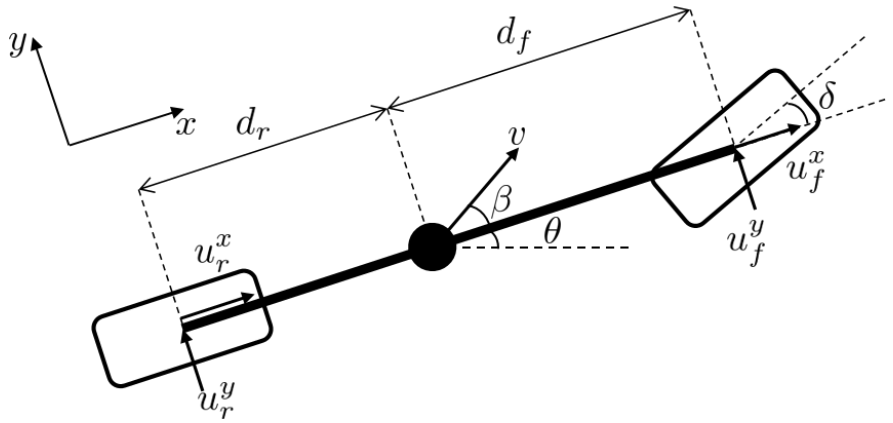

FIGURE 2.1: WMR dynamics

$$m\dot{v} = (u_f^x + u_r^x)\cos\beta + (u_f^y + u_r^y)\sin\beta \tag{2.1}$$

$$mv(\dot{\beta} + \dot{\theta}) = -(u_f^x + u_r^x)\sin\beta + (u_f^y + u_r^y)\cos\beta \tag{2.2}$$

$$I_z\ddot{\theta} = d_f u_f^y - d_r u_r^y \tag{2.3}$$

$$I_w\dot{w}_r = -Ru_r^x + \tau_r^c$$

where $m \in \Re$, $I_z \in \Re$, and $I_w \in \Re$ are the WMR's mass, the moment of inertia and wheels pitch moment of inertia, respectively. The distance between each wheel and the center of mass are d_f and d_r. The x-axis and y-axis tire forces are defined as $u_j^i \in \Re$ ($i \in [x, y]$ and $j \in [f, r]$) in the body-frame. Notations i indicates x-axis and y-axis, and j indicates front and rear wheel. The rear-wheel rotation angular rate is w_r. The WMR has the same two control inputs, steering

angle and rear-wheel torque(δ, τ_r^c) as the regular rear-wheel drive mobile robot. The steering angle of the front wheel (δ) is assumed that it changes rapidly according to the control input. The rear-wheel drive torque input is defined as $\tau_r^c \in \Re$. The front wheel rotates freely without longitudinal forces.

2.2 Tire model

The tire forces of each tire u_j^i can be obtained by 'Magic formula' [19]. From the magic formula, the slip ratio κ_j, the slip angle α_j and the theoretical slip quantities s_j^i are defined as follows.

$$\kappa_j = \frac{w_j R - v_j^x}{v_j^x}, \qquad \alpha_j = \tan^{-1}(\frac{v_j^y}{v_j^x})$$

$$s_j^x = \frac{-\kappa_j}{1+\kappa_j}, \qquad s_j^y = \frac{\tan\alpha_j}{1+\kappa_j}, \qquad j \in [f, r] \tag{2.4}$$

$$s_j = \sqrt{(s_j^x)^2 + (s_j^y)^2} \tag{2.5}$$

where the quantity of s_j^x and s_j^y are the longitudinal and lateral slip quantity of j-wheel. The radius of the wheels is R. The total slip quantity of j-wheel (s_j) are calculated from the friction circle (2.5). The velocity of wheels v_j^i can be written

as below.

$$
\begin{aligned}
v_f^x &= v\cos\beta\cos\delta + (v\sin\beta + d_f\dot{\theta})\sin\delta \\
v_f^y &= -v\cos\beta\sin\delta + (v\sin\beta + d_f\dot{\theta})\cos\delta \\
v_r^x &= v\cos\beta \\
v_r^y &= v\sin\beta - d_r\dot{\theta}
\end{aligned}
$$

The quantities of v_j^x, v_j^y and w_j are the longitudinal, lateral velocity and the angular rate of j-wheel, respectively.

We assume the longitudinal and lateral forces of tires are symmetric that means the longitudinal and lateral tire forces are in the friction circle [19], and tire forces are assumed that these are linearly dependent on the vertical forces.

Tire forces can be obtained from the slip quantity (2.5). It is derived from the simplified Pacejka's Magic formula as follows [19].

$$F_j = D_t \sin(C_t \tan^{-1}(B_t s_j))F_j^z := MF(s_j) \tag{2.6}$$

$$F_j^x = \frac{s_j^x}{s_j}F_j, \qquad F_j^y = \frac{s_j^y}{s_j}F_j \tag{2.7}$$

$$F_f^z + F_r^z = mg, \qquad d_f F_f^z - d_r F_r^z = 0 \tag{2.8}$$

$$\begin{bmatrix} u_r^x \\ u_r^y \end{bmatrix} = \begin{bmatrix} F_r^x \\ F_r^y \end{bmatrix}, \qquad \begin{bmatrix} u_f^x \\ u_f^y \end{bmatrix} = \begin{bmatrix} \cos\delta & -\sin\delta \\ \sin\delta & \cos\delta \end{bmatrix} \begin{bmatrix} F_f^x \\ F_f^y \end{bmatrix} \tag{2.9}$$

where F_j is total tire forces of j-wheel, and we define equation (2.6) as $MF(s_j)$. The longitudinal and lateral forces of the j-wheel are F_j^x and F_j^y (2.7). The vertical forces of each wheel (F_j^z) are distributed of vertical forces without generating pitch moment (2.8). The quantity of B_t, C_t and D_t are tire model parameters. From magic formula definition [19], D_t is linearly related with friction coefficient μ. The friction coefficient can be obtained real-time using friction coefficient estimation algorithm [12].

2.3 Problem formulation

The WMR has three degrees of freedom (x, y, θ), whereas the WMR model just has two control input (δ, τ_r). The WMR is an under-actuated system that three DoF, and these DoF should be controlled only with two DoF. The non-holonomic constraint makes the relationship with velocity, side slip angle, and yaw rate $(v, \beta, \dot{\theta})$. However, in the slip condition, the system does not have non-holonomic constraints as in the non-slip condition. Therefore, the WMR in the slip condition is more difficult to control. In this under-actuated situation, our controller design objective is to converge WMR side slip angle (β) and yaw rate ($\dot{\theta}$) to the desired side slip angle and yaw rate. If we can change slip angle and yaw rate at will, the WMR can go through the planned path while drift-driving.

Chapter 3

Drift-Driving Control Design

In this chapter, we propose a new WMR drift-driving controller that controls the WMR to pass through the path while drift-driving. Because the WMR in slip condition is an under-actuated system without non-holonomic constraint, controlling all state is difficult while drift-driving. We concentrate on the human strategy of drift-driving. In many car drift-driving videos, we found that the human focuses on the direction of WMR. The direction of WMR is directly related to the motion of side slip angle and yaw rate, not velocity. If we control the direction of the WMR appropriately, the WMR goes through the path while drift-driving. The new drift-driving controller deals with side slip angle and yaw rate.

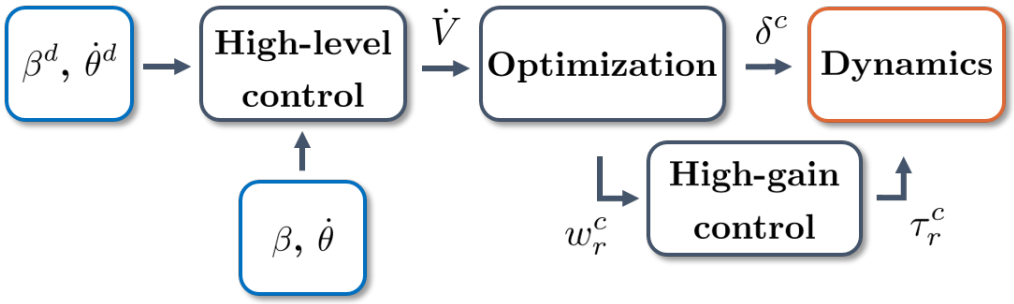

FIGURE 3.1: Flow chart

The new controller consists of the three steps as the high-level virtual control, optimization with constraints and high-gain control. The flow chart of this controller is in Fig. 3.1.

In the high-level control, set the cost function from the current side slip angle, desired slip angle, yaw rate and desired yaw rate. We obtain the derivative of cost function from the model dynamics from Section 2.1. In the optimization, minimize the derivative of cost function with tire model constraints from Section 2.2. In the high-gain control, calculate the rear-wheel torque from the results of optimization. As the result, we obtain control input δ^c and τ_r^c.

3.1 High-level control

The high-level control sets the cost function from the current side slip angle, yaw rate, desired side slip angle and desired yaw rate. This cost function is for

control the WMR from a current side slip angle and yaw rate to desired side slip angle and desired yaw rate ($[\beta, \dot{\theta}] \rightarrow [\beta^d, \dot{\theta}^d]$). The error $e \in \Re^{2\times 1}$ is defined as follows.

$$e = \begin{bmatrix} e_\beta \\ e_{\dot{\theta}} \end{bmatrix} = \begin{bmatrix} \beta - \beta^d \\ \dot{\theta} - \dot{\theta}^d \end{bmatrix}, \qquad \dot{e} = \begin{bmatrix} \dot{\beta} - \dot{\beta}^d \\ \ddot{\theta} - \ddot{\theta}^d \end{bmatrix}$$

where β^d and $\dot{\theta}^d$ are desired side slip angle and desired yaw rate of the WMR. We set a cost function V to stabilize the error.

$$V = \frac{1}{2} e^T W e, \qquad W = \begin{bmatrix} w_\beta & 0 \\ 0 & w_{\dot{\theta}} \end{bmatrix} \succeq 0$$

where W is a weight diagonal matrix about control gain. We obtain the derivative of the cost function as follows.

$$\dot{V} = -e^T W \dot{e}$$

To make the errors converges to zero, $\dot{V}$ should be lower than zero. the quantity of $\dot{V}$ is minimized by optimization in the next section.

From dynamics equations (2.2) and (2.3), above derivative of the cost function can be expressed as follows.

$$\dot{V}(u_f, u_r) = -e^T W \begin{bmatrix} \frac{-(u_f^x + u_r^x)\sin\beta + (u_f^y + u_r^y)\cos\beta}{mv} - \dot{\theta} - \dot{\beta}^d \\ \frac{d_f u_f^y - d_r u_r^y}{I_z} - \ddot{\theta}^d \end{bmatrix} \tag{3.1}$$

$u_f = [u_f^x, u_f^y]^T$ and $u_r = [u_r^x, u_r^y]^T$ are the tire forces on the front wheel and the rear wheel from the tire model. In the next section, we choose best forces that minimize $\dot{V}$ with satisfying tire model constraints.

3.2 Optimization

The slip quantity (2.4) and tire model constraints (2.9) are calculated as follows. The magic formula tire model function (MF) is defined in equation (2.6). Because the current side slip angle and yaw rate $(\beta, \dot{\theta})$ are given, The front tire forces are only the function of steering angle (δ), and the rear tire forces are only the function of rear wheel angular velocity (w_r).

$$
\begin{aligned}
s_f(\delta) &= \frac{d_f\dot{\theta}\cos\delta + v\sin(\beta-\delta)}{d_f\dot{\theta}\sin\delta + v\cos(\beta-\delta)} \\
s_r^x(w_r) &= \frac{v\cos\beta - w_r r}{w_r r}, \qquad s_r^y(w_r) = \frac{v\sin\beta - d_r\dot{\theta}}{w_r r} \\
s_r(w_r) &= \sqrt{s_r^x(w_r)^2 + s_r^y(w_r)^2}
\end{aligned}
$$

$$\begin{bmatrix} \left| \begin{bmatrix} -\sin\delta \\ \cos\delta \end{bmatrix} (-sgn(s_f(\delta))MF(|s_f(\delta)|)) - u_f \right| \\ \left| \begin{bmatrix} s_r^x(w_r) \\ s_r^y(w_r) \end{bmatrix} (-MF(s_r(w_r))\frac{1}{s_r(w_r)}) - u_r \right| \end{bmatrix}$$
$$:= T_c(u_f, u_r, \delta, w_r) \leq \begin{bmatrix} \epsilon_f \\ \epsilon_r \end{bmatrix} \tag{3.2}$$

where longitudinal slip has not occurred in the front wheel. We assumed that obtained tire model has bounded errors ϵ_f and ϵ_r. The function of sgn is the signum function.

Solve optimization minimize $\dot{V}$ (3.1) to obtain control input with the tire model constraint (3.2). The minimum $\dot{V}$ means that errors (e) converge faster than other control input.

$$U^c = \begin{bmatrix} \delta^c \\ w_r^c \end{bmatrix} = \underset{\delta, w_r}{\operatorname{argmin}} \quad \dot{V}(u_f, u_r) \tag{3.3}$$

subject to

$$T_c(u_f, u_r, \delta, w_r) \leq \epsilon, \qquad |\delta| \leq \delta_{max}$$

where δ_{max} is the positive max steering angle. To reduce the computation time of solving this optimization (3.3), we simplify its constraints.

In the tire model constraints (3.2), u_f and u_r can be expressed as the function of δ, w_r and γ.

$$\begin{aligned} u_f(\delta, \gamma_f) &= \begin{bmatrix} -\sin\delta \\ \cos\delta \end{bmatrix} (-sgn(s_f(\delta))MF(|s_f(\delta)|)) + \gamma_f \\ u_r(w_r, \gamma_r) &= \begin{bmatrix} s_r^x(w_r) \\ s_r^y(w_r) \end{bmatrix} (-MF(s_r(w_r)))\frac{1}{s_r(w_r)}) + \gamma_r \\ |\gamma| &\leq \epsilon \end{aligned} \tag{3.4}$$

where $\gamma = [\gamma_f, \gamma_r]^T$ are error parameters about tire model. From this simplified constraint (3.4), $\dot{V}$ is expressed the function of δ, w_r. The simplified optimization problem is as follows.

$$U^c = \begin{bmatrix} \delta^c \\ w_r^c \end{bmatrix} = \underset{\delta, w_r, \gamma}{\operatorname{argmin}} \quad \dot{V}(\delta, w_r, \gamma) \tag{3.5}$$

subject to

$$|\gamma| \leq \epsilon \qquad |\delta| \leq 45^\circ$$

The result of U^c is the optimized rear-wheel angular velocity and steering angle control input. These control inputs are converted to rear-wheel torque and

steering angle in the next section.

3.3 High-gain control

The control steering input and rear-wheel rotation rate (δ^c, w_r^c) are obtained in (3.5). Since the WMR's control inputs are steering angle and rear-wheel torque (δ^c, τ_r^c), the high-gain control is applied in order to change current rear-wheel rotation rate (w_r) to calculated control rear-wheel rotation rate (w_r^c). The input torque τ_r^c is calculated as follows.

$$\begin{aligned} I_w \dot{w}_r &= -R u_r^x + \tau_r \\ \tau_r^c &= R u_r^x - K_\tau \ \mathrm{sgn}(w_r - w_r^c) \end{aligned} \tag{3.6}$$

where the moment of inertia of tire is I_w. The current wheel x-axis friction force u_r^x is obtained from tire model. The high-gain control input is τ_r^c.

Chapter 4

Analysis of Control

4.1 Internal dynamics

The proposed controller controls the WMR drift-driving with three values $(v, \beta, \dot{\theta})$ only with control two values the side slip angle and yaw rate $(\beta, \dot{\theta})$. The internal dynamics of the WMR is the velocity dynamics (v). Since the proposed controller's control input is obtained from optimization, we can not determine the real control input of the controller. We analyze the internal dynamics using zero dynamics with Jacobian linearization. Assuming the side slip angle and yaw rate (β,$\dot{\theta}$) can converges to desired side slip angle and desired yaw rate(β^d, $\dot{\theta}^d$)

using proposed controller.

$$
\begin{aligned}
x &= \begin{bmatrix} v & \beta & \dot{\theta} \end{bmatrix}^T \qquad \nu = \begin{bmatrix} \delta & w_r \end{bmatrix}^T \\
e_x &= x - x^{eq} = \begin{bmatrix} e_1 & e_2 & e_3 \end{bmatrix}^T \\
e_\nu &= \nu - \nu^{eq}
\end{aligned}
$$

where x is the vector of velocity, side slip angle and yaw rate. The error between the vector x of current and equilibrium is e_x, and the error between current and equilibrium control input is e_v. From WMR dyanmics (2.1)-(2.3), The derivative of x ($f(x, \nu)$) is defined as follows.

$$
\dot{x} = f(x, \nu) = \begin{bmatrix} \frac{1}{m}((u_f^x + u_r^x)\cos\beta + (u_f^y + u_r^y)\sin\beta) \\ \frac{1}{mv}(-(u_f^x + u_r^x)\sin\beta + (u_f^y + u_r^y)\cos\beta) - \dot{\theta} \\ \frac{1}{I_z}(d_f u_f^y - d_r u_r^y) \end{bmatrix}
$$

$$
\begin{aligned}
\dot{x}^{eq} &= f(x^{eq}, \nu^{eq}) = 0 \\
\dot{x} - \dot{x}^{eq} &= f(x, \nu) - f(x^{eq}, \nu^{eq}) \\
&= A(x - x^{eq}) + B(\nu - \nu^{eq}) + H.O.T \\
\dot{e}_x &\approx Ae_x + Be_\nu \\
A &= \left.\frac{\partial f(x,\nu)}{\partial x}\right|_{x^{eq},\nu^{eq}} = \begin{bmatrix} A_1 \\ A_2 \\ A_3 \end{bmatrix} \in R^{3\times 3} \\
B &= \left.\frac{\partial f(x,\nu)}{\partial \nu}\right|_{x^{eq},\nu^{eq}} = \begin{bmatrix} B_1 \\ B_2 \\ B_3 \end{bmatrix} \in R^{3\times 2}
\end{aligned}
$$

where matrix A and B are jacobian linearized dynamics matrix. The objective of control input e_ν makes the side slip angle and yaw rate $(\beta, \dot{\theta})$ converge to the desired $(\beta^d, \dot{\theta}^d)$. The control input e_ν can be obtained as values for making $\begin{bmatrix} \dot{\beta} & \ddot{\theta} \end{bmatrix}^T$ to $-K \begin{bmatrix} \beta - \beta^d & \dot{\theta} - \dot{\theta}^d \end{bmatrix}^T$ where $K \in \Re^{2\times 2}$. If the control input works properly, e_v can be expressed as below. Desired side slip angle and yaw rate can

be an equilibrium point ($\beta^d = \beta^{eq}, \dot{\theta}^d = \dot{\theta}^{eq}$).

$$K_x = \begin{bmatrix} 0_{2\times 1} & K \end{bmatrix} \in \Re^{2\times 3}$$
$$-K_x e_x = \begin{bmatrix} A_2 \\ A_3 \end{bmatrix} e_x + \begin{bmatrix} B_2 \\ B_3 \end{bmatrix} e_v$$
$$e_\nu = -\begin{bmatrix} B_2 \\ B_3 \end{bmatrix}^{-1} (K_x + \begin{bmatrix} A_2 \\ A_3 \end{bmatrix}) e_x$$

where the control input errors e_v is calculated from current side slip angle error and yaw rate error (e_2, e_3).

$$\dot{e}_x = Ae_x + Be_\nu = Ae_x - B\begin{bmatrix} B_2 \\ B_3 \end{bmatrix}^{-1} (K_x + \begin{bmatrix} A_2 \\ A_3 \end{bmatrix}) e_x$$

As the result,

$$\dot{e}_1 = A_1 e_x - B_1 \begin{bmatrix} B_2 \\ B_3 \end{bmatrix}^{-1} (K_x + \begin{bmatrix} A_2 \\ A_3 \end{bmatrix}) e_x \tag{4.1}$$

e_2 and e_3 go to zero with controller. $(e_2, e_3 \to 0)$.

$$\dot{e}_1 = (A_{1,1} - B_1 \begin{bmatrix} B_2 \\ B_3 \end{bmatrix}^{-1} \begin{bmatrix} A_{2,1} \\ A_{3,1} \end{bmatrix}) e_1 = F e_1 \tag{4.2}$$

To analyze the stability of v, we choose many equilibrium points at side slip angle grid and yaw rate grid. The stability of v is determined by F. If F is less than zero, the velocity state of the equilibrium point is stable. If not, the velocity state of the equilibrium is unstable. We can choose the desired side slip angle and yaw rate base on F value. If F is less than 0, which uncontrolled velocity can converge in near equilibrium points.

4.2 Stability analysis

In this section, we analyze the stability of the drift-driving controller. The control objective is converging side slip angle and yaw rate (β, $\dot{\theta}$) to desired side slip angle and yaw rate (β^d, $\dot{\theta}^d$). The contours of $\dot{V}$ on the siumlation with parameter with TABLE 5.1 are exists in Fig. 4.1, Fig. 4.2.

The control input is chosen from optimization of minimizing $\dot{V}$. If $\dot{V}$ always smaller than zero, the side slip angle and yaw rate goes to the desired values. Many of the states can generate control input to make $\dot{V} \leq 0$ in the simulation at the Chapter 5.

A control input, however, may not exist to make $\dot{V} \leq 0$ because of the uncontrolled velocity dynamics. We can express the side slip angular rate from the equation (2.2) as follows.

$$\dot{\beta} = \frac{-(u_f^x + u_r^x)\sin\beta + (u_f^y + u_r^y)\cos\beta}{mv} - \dot{\theta}$$

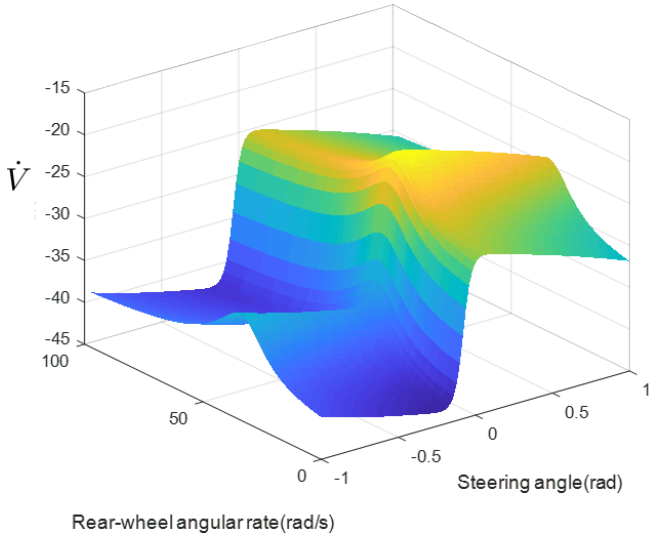

FIGURE 4.1: The contours of $\dot{V}$

In drift-driving, the sign of side slip angle and yaw rate is different, and tire forces u_j^i are bounded by tire-model. Therefore, if the velocity is too fast, the spectrum of $\dot{\beta}$ is too narrow to make $\dot{V} \leq 0$. In this situation, we decrease the velocity if $\dot{\beta}$ is bigger than zero. From the equation (4.1), the velocity error dynamics is as

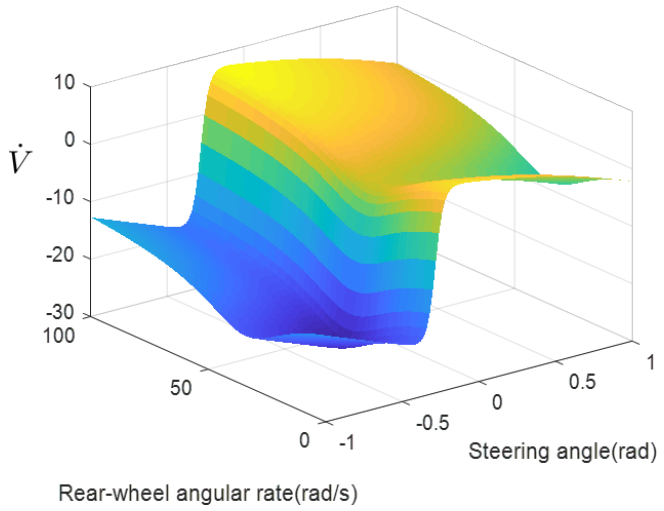

FIGURE 4.2: The contours of $\dot{V}$ (Cont)

below.

$$
\begin{aligned}
\dot{e}_1 &= A_1 e_x - B_1 \begin{bmatrix} B_2 \\ B_3 \end{bmatrix}^{-1} (K_x + \begin{bmatrix} A_2 \\ A_3 \end{bmatrix}) e_x \\
&= (A_{1,1} - B_1 \begin{bmatrix} B_2 \\ B_3 \end{bmatrix}^{-1} \begin{bmatrix} A_{2,1} \\ A_{3,1} \end{bmatrix}) e_1 + \\
&\left(\begin{bmatrix} A_{1,2} & A_{1,3} \end{bmatrix} - B_1 \begin{bmatrix} B_2 \\ B_3 \end{bmatrix}^{-1} (K + \begin{bmatrix} A_{2,2} & A_{2,3} \\ A_{3,2} & A_{3,3} \end{bmatrix}) \right) \begin{bmatrix} e_2 \\ e_3 \end{bmatrix} \\
&= F e_1 + G \begin{bmatrix} e_2 \\ e_3 \end{bmatrix}
\end{aligned}
$$

If the desired side slip angle and yaw rate are in the region where $F \leq 0$, the

velocity error e_1 converges to near equilibrium. That means if the velocity is too high and keep the side slip angle error and yaw rate error small enough, the velocity will decrease to near equilibrium $-\frac{1}{F}G[e_2, e_3]^T$. As the result, the velocity would be enough to control $\dot{V} \leq 0$. The proposed controller choose the control input to minimize $\dot{V}$ that resists the increase of side slip angle error and yaw rate error when $\dot{V}$ is bigger than 0.

More precise analysis about stability should be in the future work.

Chapter 5

Simulation Results

In this chapter, the simulated results of the proposed drift-driving controller are provided. The controller is implemented in the CarSim2016.2 simulator, which is often used to test algorithms in the vehicle area.

5.1 Simulation setup

A custom rear-wheel drive four WMR is provided in the CarSim software. It has the same parameters in TABLE 5.1 where the simulation system mass, the radius of wheels and yaw inertia are defined.

Parameters	Values
Total mass	$1650kg$
Gravity acceleration	$9.81m/s^2$
d_f	$1.4m$
d_r	$1.65m$
Radius of wheels	$0.337m$
Yaw inertia	$3234kg \cdot m^2$
B_t	14.1216
C_t	1.37107
D_t	1.05724

TABLE 5.1: The simulated WMR parameters table

The tire model Magic formula parameters of the simulation are B_t, C_t and D_t which obtained from fitting simulator tire force value given CarSim (2.6) as Fig. 5.1. The roll and pitch inertia are 928.1Kg·m^2 and 2788.5Kg·m^2, respectively. The distance between the left wheel and the right wheel is 1.6m. The hight of the mass center is 0.4m, the WMR has rear limited slip differential gear and the friction coefficient (μ) in the simulation is 0.85. The simulator runs at 1000Hz and the drift-driving controller runs at 100Hz.

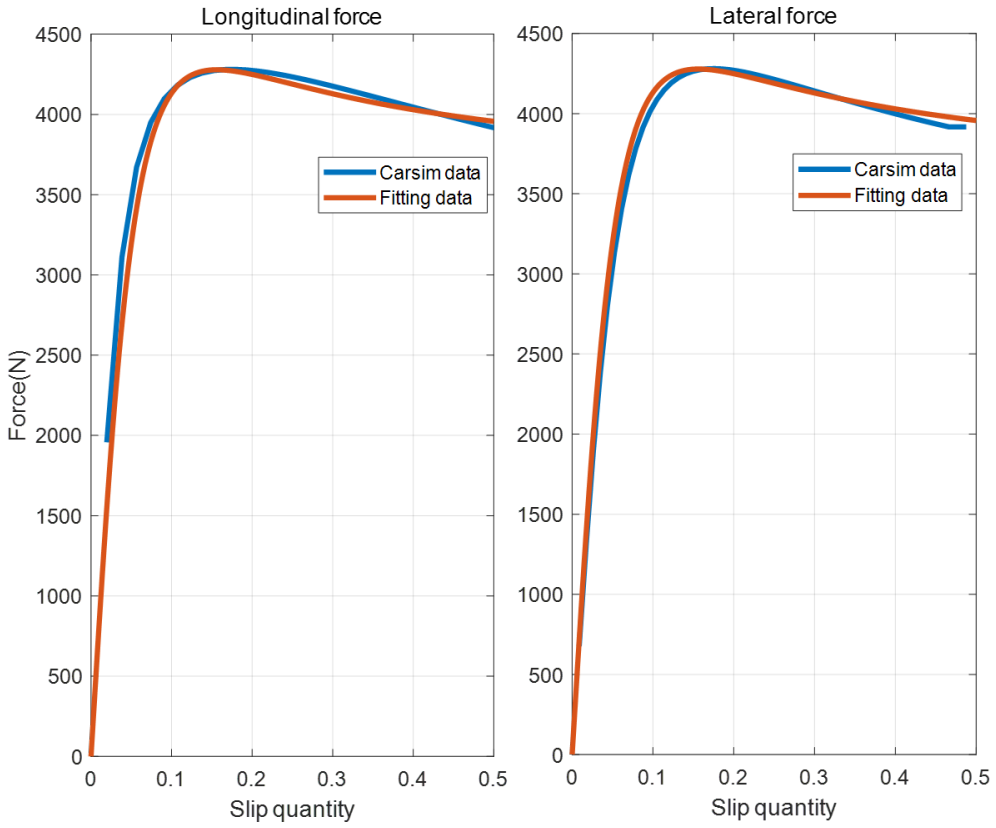

FIGURE 5.1: Fitting CarSim tire-model to simplified magic formula

5.2 Steady-state drift-driving

Steady-state equilibrium points to stabilize the uncontrolled velocity should be chosen to be the desired value. Using equation (4.2), many equilibrium points

in $-1.6 < \beta < 0$ and $0 < \dot{\theta} < 2$ are checked velocity stability with the simulation parameters. The steady-state drift-driving is simulated as Fig. 5.2.

FIGURE 5.2: An example of steady-state drift CarSim simulation

The results of the velocity stability at the equilibrium points are in Fig. 5.3. The blue points mean that the velocity at the equilibrium point is stable and the red points mean that the velocity at the equilibrium point is unstable. It also calculated with parmeters in TABLE 5.1.

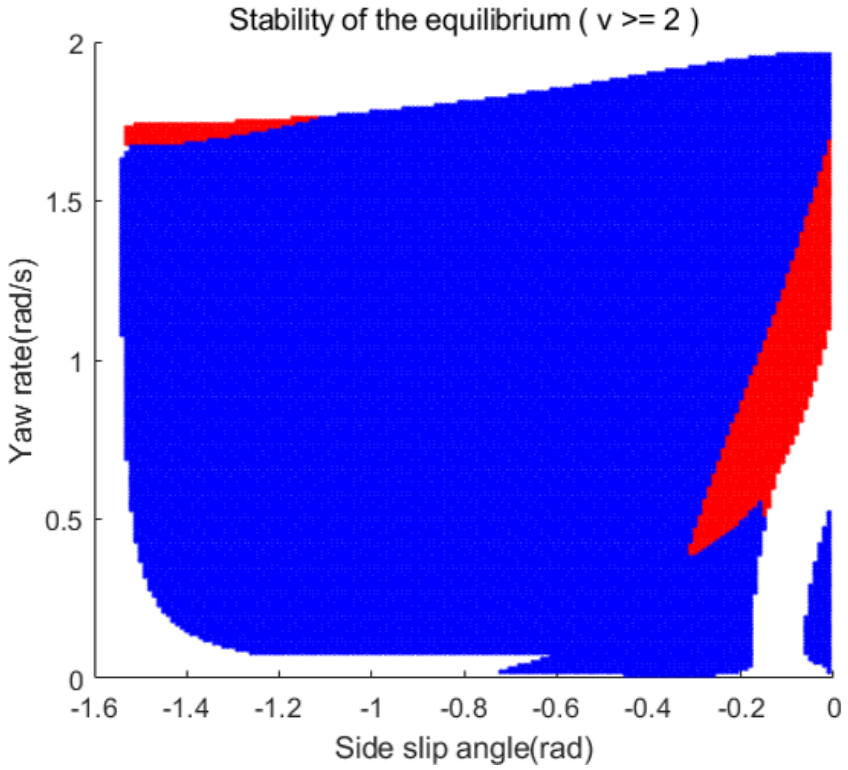

FIGURE 5.3: Linearized dynamics

The controller obtains the current velocity, side slip angle and yaw rate $(v, \beta, \dot{\theta})$. The controller gives the control input as steering angle and rear-wheel torque (δ, τ_r) to the simulator. A selected drift-driving desired side slip angle and yaw rate are $-0.4rad$ and $0.8rad/s$.

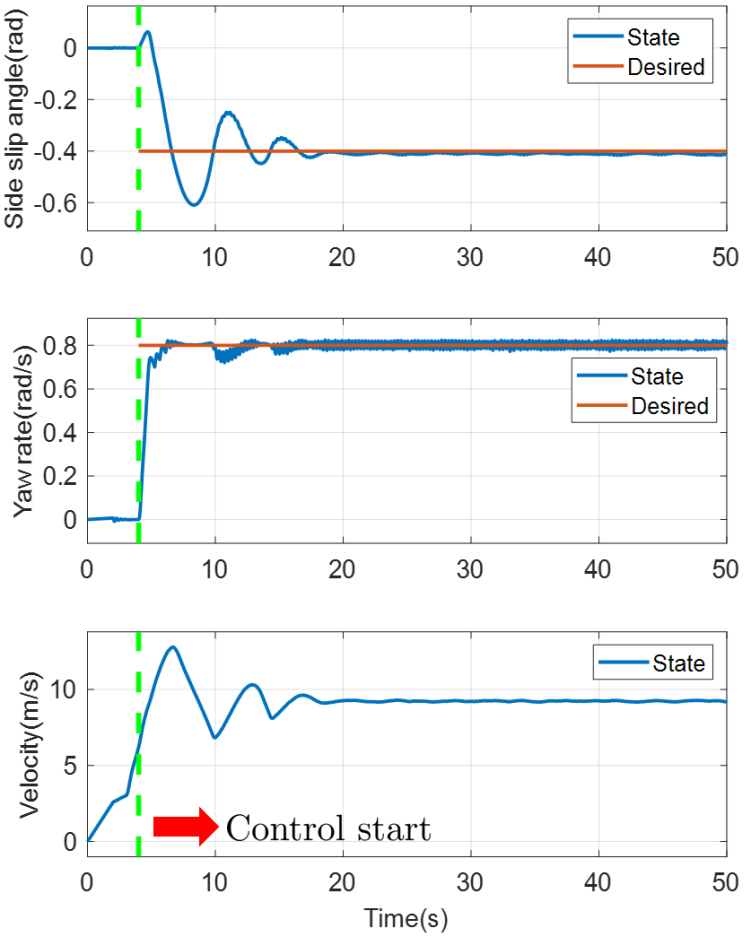

FIGURE 5.4: Carsim result plots

An example of the result of steady-state drift-driving values in CarSim simulation is provided in Fig. 5.4. The manual control input is applied from initial to four seconds. This manual input just accelerates the WMR in a straight trajectory.

After four seconds, the WMR is controlled by the proposed controller. The results show that velocity, side slip angle, and yaw rate of the WMR converge to the steady-state value. The controller converges side slip angle and yaw rate, and uncontrolled velocity converges.

Moreover, using the proposed drift-driving controller, the WMR while drift-driving can track the changing desired steady-state value. See Fig. 5.5, the desired steady-state value is changed at the 40s and 70s. The first desired side slip angle and yaw rate are $-0.7rad$ and $0.8rad/s$. The second desired side slip angle and yaw rate are $-0.5rad$ and $0.7rad/s$. The third desired side slip angle and yaw rate are $-0.4rad$ and $1.0rad/s$. The velocity, side slip angle and yaw rate converges.

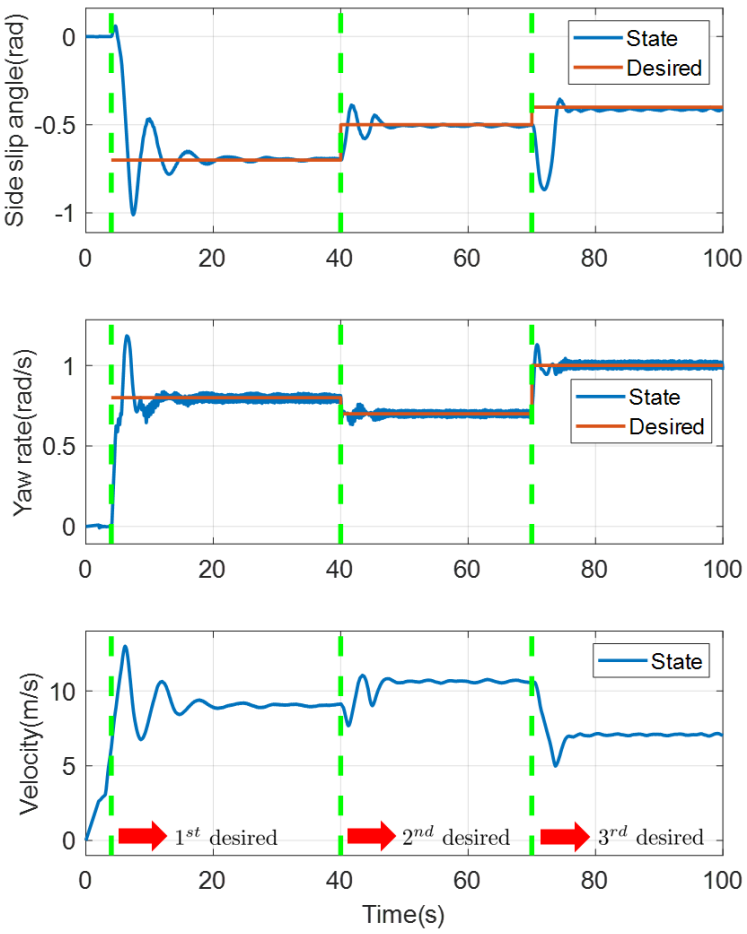

FIGURE 5.5: Carsim result plots of changing desired

5.3 Hairpin turn drift-driving

A hairpin turn is a bend in a road which necessary to turn about 180 degrees. The WMR can drive drift-driving on hairpin planned path with yaw angle using the proposed controller. The global planned path position and yaw angle is defined as ($P^g = \begin{bmatrix} x^g & y^g \end{bmatrix}^T$, θ^g). The desired side slip angle (β^d) and yaw rate ($\dot{\theta}^d$) is calculated from the planned path as follows.

$$\begin{aligned} \beta^d &= (\tan^{-1}(\frac{\dot{x}^g_{sel}}{\dot{y}^g_{sel}}) - \theta) + K_{lat}\text{sat}(\begin{bmatrix} 0 \\ 1 \end{bmatrix} (\mathbf{R}(\theta)P - \mathbf{R}(\theta)P^g_{sel})) \\ \dot{\theta}^d &= \dot{\theta}^g_{sel} - K_\theta(\theta - \theta^g_{sel}) \\ \mathbf{R}(\theta) &= \begin{bmatrix} \cos\theta & \sin\theta \\ -\sin\theta & \cos\theta \end{bmatrix} \end{aligned} \tag{5.1}$$

where the position and yaw angle of selected planned path point are P^g_{sel} and θ^g_{sel}. The selected point is a point in the path which near with current position. The rotation matrix from global frame to body frame is $\mathbf{R}(\theta)$. The current position and yaw rate of the WMR is P and θ. The saturation function is sat(). The quantities of K_{lat} and K_θ are lateral feedback gain and yaw angle error feedback gain. The desired side slip angle consists of velocity direction of current position term and lateral feedback term, and the desired yaw rate consists the selected path's yaw rate term and yaw angle feedback term.

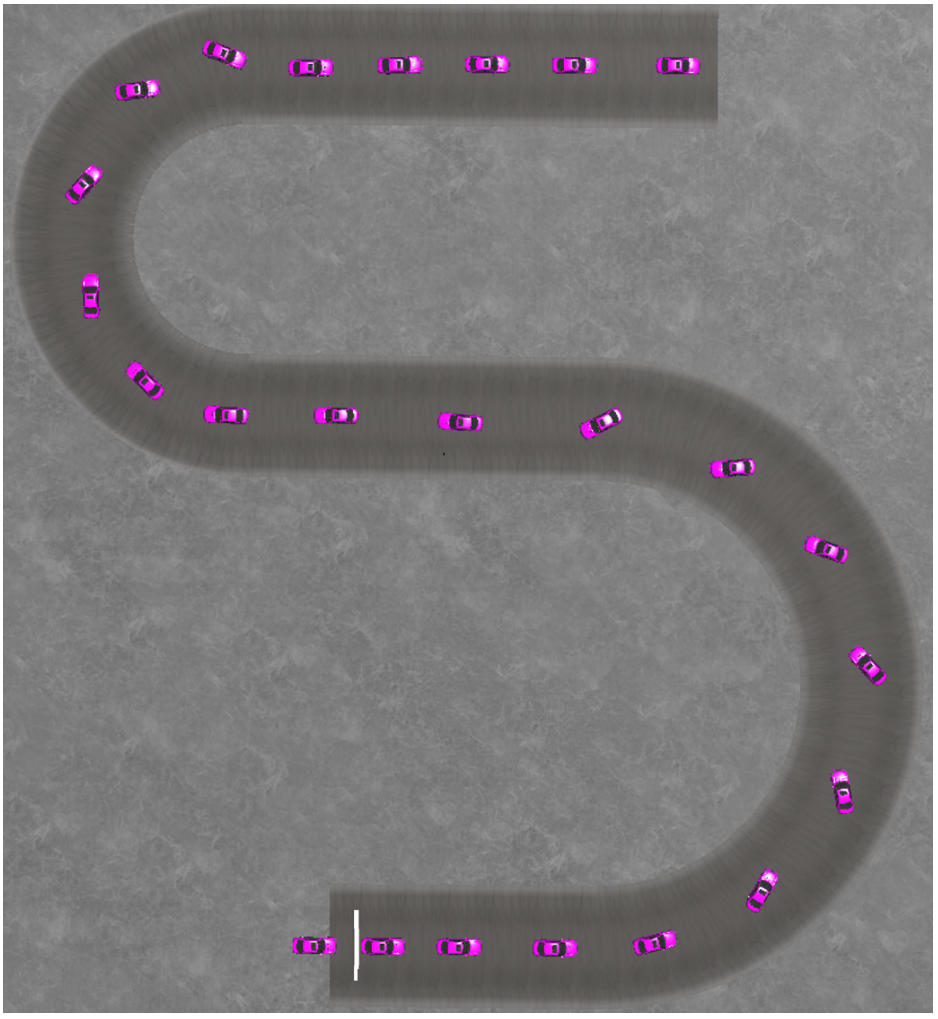

FIGURE 5.6: Carsim hairpin path simulation (Top view)

We simulate drift-driving in a hairpin path as Fig. 5.6 and Fig. 5.7. The planned path is divided by straight paths and curved paths as Fig. 5.8. The planned yaw

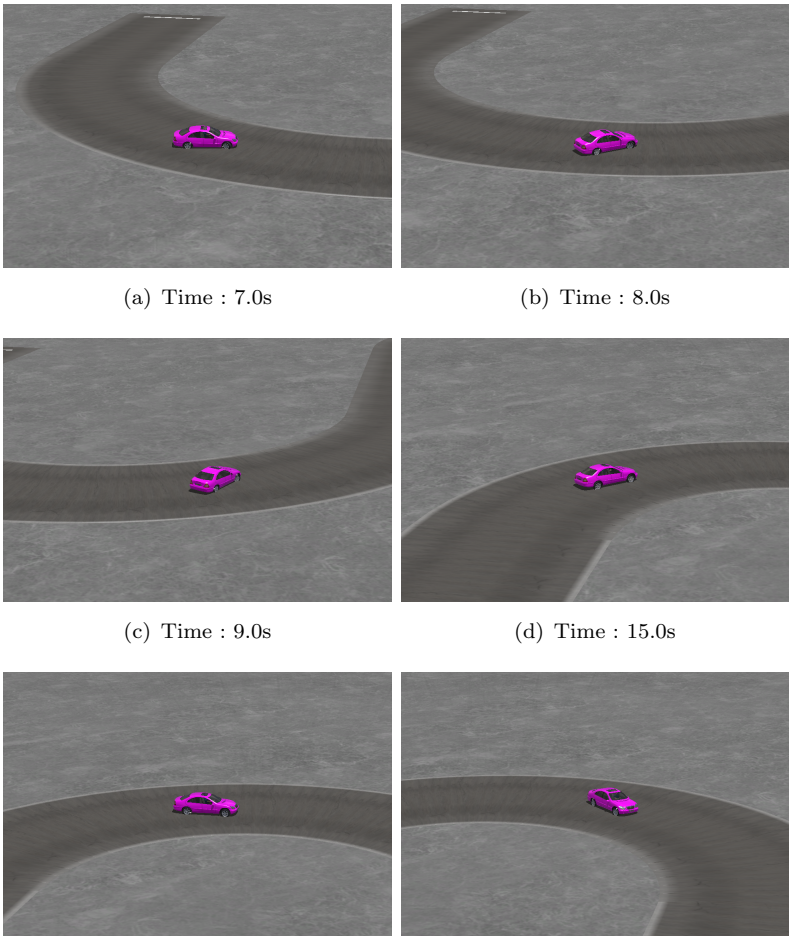

(a) Time : 7.0s (b) Time : 8.0s

(c) Time : 9.0s (d) Time : 15.0s

(e) Time : 16.0s (f) Time : 17.0s

FIGURE 5.7: Carsim hairpin turn path simulation (Side view)

angle of straight paths is the same as the direction of the planned path angle. In the first curve, the planned yaw angle is the same as the path direction angle at curve start. The angle difference between the planned yaw angle and the path

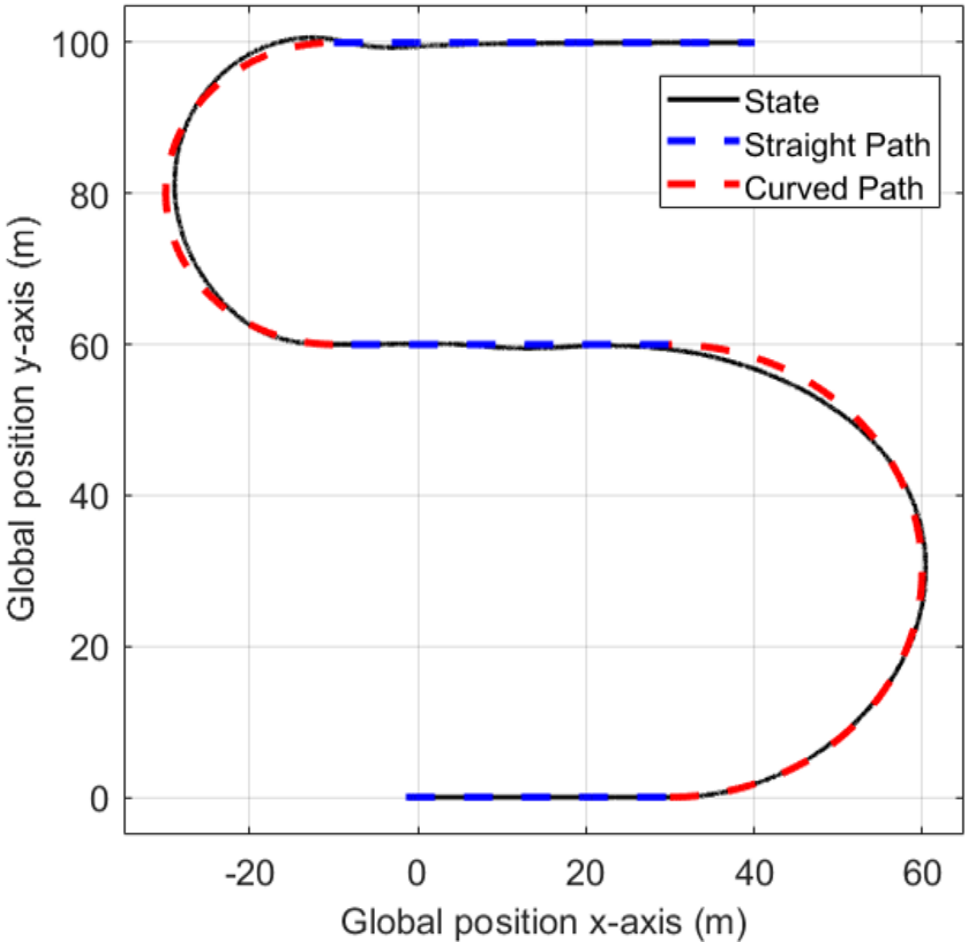

FIGURE 5.8: Carsim result position plot of hairpin desired

direction angle linearly increases from zero to $0.7rad$ on a quarter of the first curve. Between a quarter of the curve and the end of the curve, the planned yaw angle is $0.7rad$ bigger than the path direction angle. In the second curve, the planned yaw angle is the same as in the first curve only different with $0.5rad$

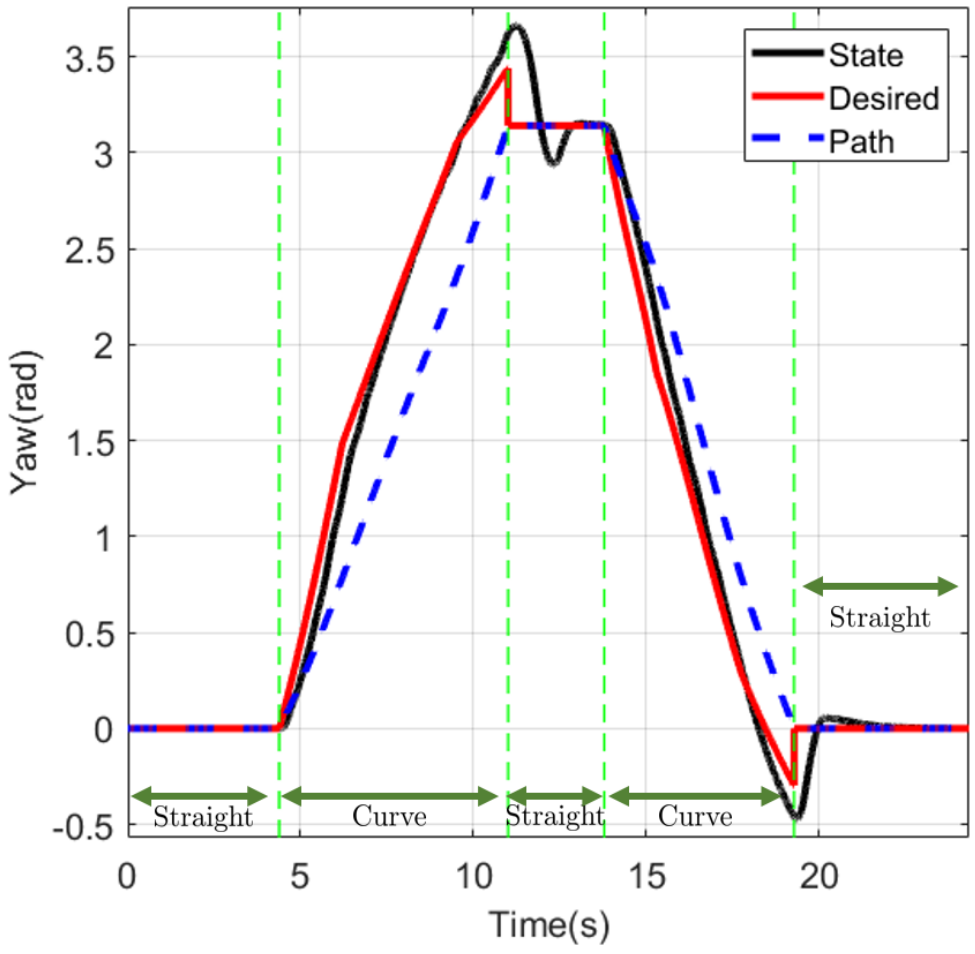

FIGURE 5.9: Carsim result yaw angle plot of hairpin desired

smaller than the path direction angle. In all curved path, we choose nearest point of the desired path as a path with same angle of curve center.

We calculate the desired side slip angle (β^d) and yaw rate ($\dot{\theta}^d$) using equation

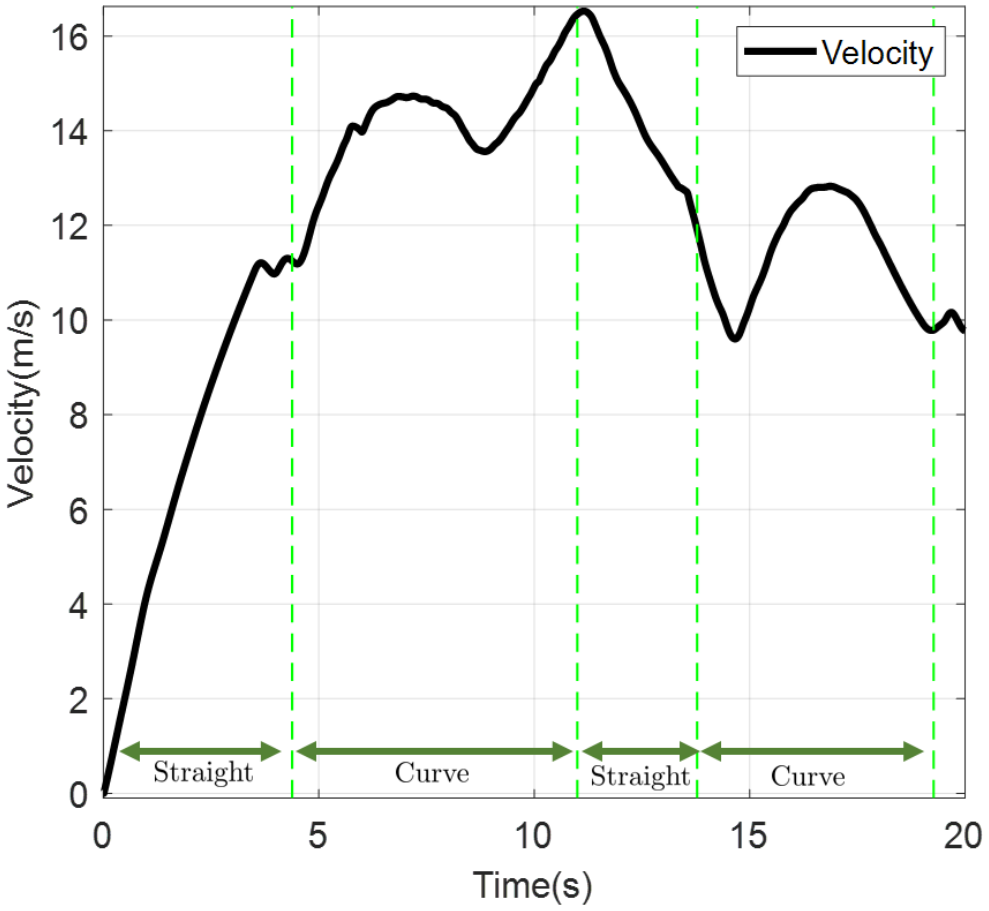

FIGURE 5.10: Carsim result velocity plot of hairpin desired

(5.1) and control WMR using the proposed controller. In all straight path, we control rear wheel for velocity to the desired velocity, and steering angle set from the position feedback using simple p-controller. The first straight path desired velocity is $11m/s$, and the second straight path desired velocity is $10m/s$.

The Fig. 5.6 is top view of the CarSim simulation. The Fig. 5.7 are side views of the CarSim simulation at t = 7.0s, 8.0s, 9.0s, 15.0s, 16.0s and 17.0s. The front three subfigures are the WMR in the first curve. The later three subfigures are the WMR in the second curve.

The hairpin path following simulation result plots are in Fig. 5.8, Fig. 5.9 and Fig. 5.10. In Fig. 5.8, the WMR follows the planned path with errors in the curved path. The WMR follows the planned yaw angle on the curved path in Fig. 5.9. The position and yaw errors at initial are small but the errors increase while drifting. Moreover, because we do not control velocity, If the velocity is too high or low, we can not generate $\dot{\beta}, \ddot{\theta}$ to converges side slip angle and yaw rate to desired values.

In steady-state drift-driving, if the velocity is too high or low, the velocity converges to the equilibrium values. But, it seriously affects on the path following. The velocity while path following should be dealt with, and it is the future work.

Chapter 6

Conclusion and Future Work

6.1 Conclusions

In this thesis, we proposed the new drift-driving controller in the WMR slip condition which has three degrees of freedom only with two control inputs. From human strategy, we concentrate on the direction of the WMR. The proposed controller controls only two states, side slip angle, and yaw rate. This controller uses the 2-wheeled WMR dynamics and the Magic formula tire model. This drift-driving control sets cost function between current and desired the side slip angle and yaw rate, and the controller optimizes to minimize derivative of this cost function to decrease errors. The drift-driving controller was tested to the steady-state drift-driving through high fidelity CarSim simulation to verify it

in Section 5.2. The stability of the uncontrolled state, velocity, and controlled state stability in equilibrium points are analyzed. Moreover, The drift-driving controller was tested to the hairpin turn drift-driving CarSim simulation which is not steady-state in Section 5.3.

6.2 Future work

Future work includes the precise stability analysis of optimization and control. In this thesis, we only analysis stability of optimization and control with linearized dynamics. Since the optimization function is non-linear, we should deal more precise stability analysis. In addition, future work includes the analysis of initial velocity for path following, too. The initial velocity is important for the path following with drift-driving adequately, because it takes a long time to converge the desired if the initial speed is too high or low. It should be analyzed that the proper initial velocity and the effects of initial velocity.

Bibliography

[1] H. Yang and D. Lee. Cooperative grasping control of multiple mobile manipulators with obstacle avoidance. In *Proc. IEEE Int'l Conf. on Robotics and Automation (ICRA)*, pages 836–841, 2013.

[2] K. Y. Lui, H. Cho, C. Ha, and D. Lee. First-person view semi-autonomous teleoperation of cooperative wheeled mobile robots with visuo-haptic feedback. *The International Journal of Robotics Research*, 36(5-7):840–860, 2017.

[3] C. Ha, J. Yoon, C. Kim, Y. Lee, S. Kwon, and D. Lee. Teleoperation of a platoon of distributed wheeled mobile robots with predictive display. *Autonomous Robots*, 42(8):1819–1836, 2018.

[4] D. Chwa. Robust distance-based tracking control of wheeled mobile robots using vision sensors in the presence of kinematic disturbances. *IEEE Transactions on Industrial Electronics*, 63(10):6172–6183, 2016.

[5] G. Williams, N. Wagener, B. Goldfain, P. Drews, J. M. Rehg, B. Boots, and E. A. Theodorou. Information theoretic mpc for model-based reinforcement learning. In *Proc. IEEE Int'l Conf. on Robotics and Automation (ICRA)*, pages 1714–1721, 2017.

[6] D. Wang and C. B. Low. Modeling and analysis of skidding and slipping in wheeled mobile robots: Control design perspective. *IEEE Transactions on Robotics*, 24(3):676–687, 2008.

[7] D. Lee. Passivity-based switching control for stabilization of wheeled mobile robots. In *Robotics: Science and Systems*, 2007.

[8] N. Seegmiller and A. Kelly. High-fidelity yet fast dynamic models of wheeled mobile robots. *IEEE Transactions on Robotics*, 32(3):614–625, 2016.

[9] Z. Zuo and D. Lee. Haptic tele-driving of a wheeled mobile robot over the internet: a pspm approach. In *Proc. IEEE Conference on Decision and Control (CDC)*, pages 3614–3619, 2010.

[10] J. Yoon, J.-H. Oh, J.-H. Park, S. Kim, and D. Lee. Autonomous dynamic driving control of wheeled mobile robots. In *Proc. IEEE Int'l Conf. on Robotics and Automation (ICRA)*, pages 5274–5279, 2014.

[11] H. Yang, S.-Y. Jeon, and D. Lee. Fast zmp and friction force calculation of mobile robot trajectory on uneven trajectory. In *Proc. Int'l Conf. on Ubiquitous Robots and Ambient Intelligence (URAI)*, pages 884–885, 2017.

[12] S.-Y. Jeon, R. Chung, and D. Lee. Tire force estimation of dynamic wheeled mobile robots using tire-model based constrained kalman filtering. In *Proc. IEEE/RSJ Int'l Conference on Intelligent Robots and Systems*, pages 2470–2477, 2018.

[13] E. Velenis, D. Katzourakis, E. Frazzoli, P. Tsiotras, and R. Happee. Steady-state drifting stabilization of rwd vehicles. *Control Engineering Practice*, 19 (11):1363–1376, 2011.

[14] R. Y. Hindiyeh and J. C. Gerdes. A controller framework for autonomous drifting: Design, stability, and experimental validation. *ASME Journal of Dynamic Systems, Measurement, and Control*, 136(5):051015, 2014.

[15] J. Y. Goh and J. C. Gerdes. Simultaneous stabilization and tracking of basic automobile drifting trajectories. In *Proc. IEEE Intelligent Vehicles Symposium (IV)*, pages 597–602, 2016.

[16] F. Zhang, J. Gonzales, S. E. Li, F. Borrelli, and K. Li. Drift control for cornering maneuver of autonomous vehicles. *Mechatronics*, 54:167–174, 2018.

[17] J. Gonzales, F. Zhang, K. Li, and F. Borrelli. Autonomous drifting with onboard sensors. In *Proc. Int'l Symp. on Advanced Vehicle Control*, page 133, 2016.

[18] E. Joa, K. Yi, and Y. Hyun. Autonomous drift control using vehicle lateral dynamics with self-rotation and revolution. In *Proc. Int'l Symp. on Advanced Vehicle Control*, 2018.

[19] E. Bakker, H. B. Pacejka, and L. Linder. A new tire model with an application in vehicle dynamics studies. In *Proc. Autotechnologies Conference and Exposition*, pages 83–95, 1989.

요약

본 논문에서는 Wheeled Mobile Robot(WMR)의 자율 드리프트 드라이빙 컨트롤러를 디자인 하고 분석하며, 이를 상용 프로그램인 CarSim을 사용한 시뮬레이션을 통하여 알고리즘을 검증 한다. 첫째로, WMR의 다이나믹스와 타이어 모델을 정의하고, 이러한 모델로 인한 제약 사항에 대하여 논의한다. 다음으로, 사람의 관점에서 드리프트 드라이빙을 분석하고, 드리프트 드라이빙 제어기의 제어 목적을 정의한다. (차량의 방향과 요 각속도를 제어한다.) 드리프트 드라이빙 제어기는 고-레벨 제어, 목표 값을 찾기 위한 최적화 그리고 고-게인 제어로 구성된다. 다음으로, 제어하지 않는 속도에 대한 분석을 진행 하였다. 마지막으로 제안한 알고리즘을 CarSim 시뮬레이터를 이용하여 검증하였다. 정상 상태의 드리프트 시뮬레이션 결과와, 헤어핀 경로에 대한 드리프트 시뮬레이션 결과를 제시 한다.

주요어: Wheeled Mobile Robot, Drift-driving control, Tire-model, Optimization, High-gain control, Jacobian linearization

학번: *2017-23468*